Nanolimes doped with Quantum Dots for stone consolidation assessment

Javier Becerra[1], Pilar Ortiz[1], José María Martín[1], Ana Paula Zaderenko[1]

[1]Departamento de Sistemas Físicos, Químicos y Naturales, Universidad Pablo de Olavide, Ctra. Utrera Km1, ES-41013, Seville, Spain.

[*]Corresponding author: J. Becerra: jbeclun@upo.es

Abstract

Currently, the application of consolidation treatments based on nanolimes ($Ca(OH)_2$ nanoparticles) has become a common practice during the restoration of historical buildings. However, recent studies have showed that their effectiveness on stone materials is lower than expected. This result is due to the accumulation of nanolimes near the surface, which decreases their depth penetration into stone matrix and, consequently, results in a low restoration effectiveness.

This research is focused in a new nanocomposite based on $Ca(OH)_2$ nanoparticles decorated with ZnO quantum dots whose fluorescence shows the real penetration of the nanomaterial into the stone matrices and allows us to study the affinity between nanolimes and the solvent used in the application in order to improve the penetration of the treatment in stones. Different mixtures of solvents have been probed to improve the surface depth penetration by analysing their kinetic stabilities and using thin-layer chromatography to evaluate their capacity to transport the nanolimes. Furthermore, a new support for thin-layer chromatography based on mortar has been

designed, which has the advantage of having the same chemical composition as the limestones. Moreover, the effectiveness of the treatments was studied on limestones from Puerto de Santa María and Espera (Spain), which have been widely used in historical and contemporary buildings in the southwest of Spain.

Nanolimes doped with ZnO quantum dots allow one to choose the optimal solvents for each kind of stone based on their fluorescence from UV radiation. Additionally, the fluorescence of the quantum dots could be used as an indicator of the consolidated areas for cultural heritage applications.

Keywords

Stone consolidation, nanolimes, depth penetration, ZnO quantum dots

1. Introduction

One of the most common decays on historical stone buildings is the loss of cohesion of the stone matrices due to powdering, sanding, scaling or alveolation processes, all of which decrease the buildings' mechanical strength and diminish their original shapes. For that reason, restorers usually apply consolidation treatments during the restoration or intervention of monuments to try to recover the cohesion of the deteriorated stones. These treatments must satisfy several general requirements: compatibility with the original materials and effectiveness in improving the mechanical strength and durability [1,2]. However, the current consolidation treatments often lack of some of these requirements. For example, in the case of limestones, polymeric consolidants such as epoxy resins or acrylics normally are incompatible with the stone substrate (leading to strong alteration of stone porous systems, yellowing, biodeterioration, etc.) [3–6]. Silica-based consolidants, such as the widely used tetraethyl orthosilicate (TEOS) or ethyl silicate, have a low compatibility and durability despite their high penetration through the porous systems of the stone [7,8]. Finally, inorganic consolidants, such as limewater, are highly compatible with the original material and have good durability, although they have poor penetration and low effectiveness [5,6,9,10].

New formulations from the nanotechnological field have enabled improving the properties of traditional inorganic consolidants. Nanolimes are colloidal dispersions of calcium hydroxide nanoparticles, which have the advantages of limewater (compatibility and durability) and a smaller size (between 50-600 nm), which enhance the penetration through the stones' porous systems [11,12]. The effectiveness of nanolimes as a consolidation treatment has been probed in some monuments, thus achieving a good pre-consolidation over different materials, especially mural paintings and stones [6,7,13–15]. Nevertheless, this treatment often shows a poor effectiveness when mass consolidation is required since it generates a white haze on the surface [8,16–18]. According to recent studies [1,8], this phenomenon is due to the back migration of the nanoparticles to the surface during the evaporation of the solvent. This approach suggests that the choice of the solvent is fundamental to improving the penetration of the nanoparticles

through the decayed stone. Borsoi et al. [19] proposes a relation between stones' porous sizes and the kinetic stability of the dispersion to favour the precipitation of the nanoparticles at the end of the absorption process, thus preventing their back migration to the surface.

In this research, we have clarified the behaviours of the colloidal dispersion of nanolimes by studying the kinetic stability of different solvents. The affinity of the nanoparticles to the solvent or the substrate was studied using a chromatography assay and using two different substrate materials based on silica or lime. Furthermore, a selection of the different colloids that were studied was probed in limestone from Puerto de Santa María and Espera (Spain), which present substantial differences in their physical properties. These limestones were widely used in historical building, such as the important town hall [20] and the cathedral [21] of Seville (Spain) and are employed currently as construction materials.

With this objective, the nanolimes were decorated with zinc oxide quantum dots (ZnO QDs). QDs have a high luminescent efficiency [22] and have a wide variety of applications, such as in nanosensors, cosmetic products, nano-electronics, nano-optical devices and energy storage [23,24]. Moreover, ZnO QDs are stable, nontoxic and low cost [23,25], and these and other characteristics allow us to choose them as building treatments to evaluate the real depth penetration of the nanolime treatment.

2. Materials and Methods

2.1. Synthesis of $CaOH_2$ nanoparticles decorated with ZnO quantum dots

Zinc acetate ($Z_nC_4H_6O_4$), potassium hydroxide (KOH) and (3-aminopropyl)trimethoxysilane (APTES) were purchased from Sigma-Aldrich, tetraethylorthosilicate (TEOS) from Acros and calcium hydroxide nanoparticles ($Ca(OH)_2$ Nanorestore®) from CTS. All other chemicals were reagent grade. Water was purified using a Milli-Q reagent grade water system from Millipore.

ZnO quantum dots were synthesized according to the method described by Patra et al. [25] with some modifications. Briefly, a methanol solution of KOH (10 mL, 2.5 M) was added to a

methanol solution of zinc acetate (25 mL, 0.1 M) under magnetic stirring. Immediately after, 25 mL of Nanorestore® (isopropanol solution of $Ca(OH)_2$ nanoparticles at the concentration of 5 g/L) was added, and the resulting colloid was magnetically stirred for 1 h. The formation of ZnO quantum dots shows bright yellow-green luminescence under UV excitation. At this point, 250 µL of TEOS solution and 500 µL of water were added to control the quantum dot growth. After the reaction, the pellets with the nanolimes decorated with ZnO quantum dots were recovered by centrifugation (5000 rpm, 10 min), which made resuspending the pellets in an isopropanol solution easy. The isopropanol dispersion of colloids was stored in the dark until being applied over stone samples.

One modification was carried out by adding 250 µL of APTES instead of TEOS in the synthesis process. Thereby, two different nanolimes decorated with ZnO quantum dots were synthesized and named according to the stabilized products: $Ca(OH)_2$/ZnO@TEOS and $Ca(OH)_2$/ZnO@APTES.

The nanocomposites were characterized by scanning electron microscope equipped with energy-dispersive X-ray spectroscopy (SEM–EDS) and fluorescence spectroscopy. SEM images were recorded with a GeminiSEM 300 microscope, and EDS was carried out with an Oxford Instruments Detector EDS X-Max 50. The fluorescence spectra were recorded using an Ocean Optics USB2000 + fluorimeter, a 100 W xenon arc with an arc lamp power supply model LSN152, and a lamp housing model LSH102, which were all provided by Lot Oriel.

2.2. Kinetic stability assay

The kinetic stability of the nanolimes is a decisive factor for understanding their precipitation process during their depth penetration in limestones, according to research carried out by Borsoi et al. [26]. For that study, $Ca(OH)_2$ nanoparticles and $Ca(OH)_2$ nanoparticles decorated with ZnO DQs were studied as the first step to understanding their behaviours on the limestone substrates. The solvents used in the kinetic stability assay were water, ethanol, isopropanol, octanol, dimethyl sulfoxide, dimethylformamide, acetone, ethyl acetate, dipentene, toluene and

113 hexane (ordered from highest to lowest polarity), and their main characteristics are illustrated in
114 Table 1.

115 Table 1. Physical-chemical properties of the selected solvents [27–30]

Solvent	***Viscosity at 25°C (mPas)***	***Surface tension at 20°C (mN m^{-1})***	***Boiling point (°C)***	***Vapour pressure at 25°C (kPa)***	***Evaporation rate (butyl acetate=1)***	***Relative permitti-vity***	***Polarity parameter, $E_T(30)$ (Kcal mol^{-1})***	***TWA 8 h, NIOSH* (ppm)***
Water	0.8949	71.97	99.61	-	-	80.4	63.1	-
Ethanol	1.263	21.99	78.4	5.9466	2.0	24.30	51.9	1000
Isopropanol	2.1	21.40	82.2	4.1	2.90	18.60	48.6	400
Octanol	7.363	26.92	204.0	0.009	0.01	10.34	48.3	-
Dimethyl sulfoxide	1.991	42.98	189.0	0.08166	0.03	46.45	45.0	-
Dimethylformamide	0.802	37.9	153.0	0.492	3.7	-	43.8	10
Acetone	0.3029	22.68	56.1	30.8	6.60	20.56	42.2	250
Ethyl acetate	0.426	23.75	77.1	11.46	4.10	6.02	38.1	400
Dipentene	0.923	26.87	176.0	0.2667	0.20	2.38	-	-
Toluene	0.54 (20°C)	29.6	110.6	20 (18.4°C)	-	2.4	33.9	200
Hexane	0.294	17.94	68.7	20.17	6.82	1.88	30.9	50

*The time-weighted average concentration for a conventional 8-hour workday and 40-hour workweek exposure to a substance, to which it is believed that nearly all workers may be repeatedly exposed, day after day, without adverse health effects. The data are given by National Institute for Occupational Safety and Health (NIOSH).

116

117 The kinetic stabilities of the colloids were determined by turbidity measurements. The
118 absorbance at 600 nm was considered as the parameter proportional to the turbidity of the
119 dispersion, and its value decreases over time due to particle agglomeration and settling. The
120 measures were recorded by a UV-Vis spectrophotometer (Ocean Optics spectrometer equipped
121 with a HR4000 detector) at different times (0, 0.5, 1, 1.5, 3, 24 and 48 h). The kinetic stability
122 time was considered for the period until the total decantation of the dispersion, namely, until the
123 absorbance values of its supernatant liquid were stable and continuous.

124 For this assay, the different nanoparticles were centrifuged at 5000 rpm for 10 minutes and
125 resuspended in each of the solvents. These colloids were diluted in the same solvent at the ratio
126 of 1:5 and placed in 3 mL glass test tubes, which were capped to avoid the solvents'
127 evaporation. The colloids were sonicated at the beginning of the assay for 30 minutes to avoid
128 nanoparticle aggregation.

129 **2.3. Chromatography assays**

Chromatography in the liquid phase was carried out to analyse the affinity between the nanoparticles and the different solvents in different substrates. Thin-layer chromatography (TLC) was performed on aluminium plates that were pre-coated with silica gel (TLC-sheets Alugram® Sil G/UV_{245}). The size of the plates was 4.5 x 1 cm. Moreover, new chromatography plates based on mortar were designed with the main objective to analyse this phenomenon in a substrate more similar to limestone. To prepare those plates, microscope slides of 76 x 26 mm were sanded and scratched, and a thin layer of lime and sand mortar was extended along the plate length. The mortars were dried at room temperature for few weeks.

Chromatography was performed via the capillarity of the colloidal dispersions. Briefly, the initial suspensions of nanoparticles were centrifuged at 5000 rpm for 10 min and then resuspended in the following solvents (water, ethanol, isopropanol, acetone and dipentene) according to the results of the kinetic stability assay. Additionally, these colloids were diluted in the same solvent at the ratio of 1:1 in order to reach a final concentration of nanolimes of 2.5 g/L. The dissolutions were stirred for 15 min.

The distance travelled relative to the solvent (R_f) was calculated according to equation 1.

$$Rf = \frac{distance\ travelled\ by\ compound}{distance\ travelled\ by\ solvent} \qquad \text{Eq. 1}$$

2.4. Treatment evaluation scheme

Figure 1 shows a scheme of the methodology followed for the treatment evaluation of the consolidates for historical buildings and archaeological stone materials. These schemes are divided in two phases.

Phase 1: It is a preliminary trial to study the depth penetration and carbonation process of silica-coated ZnO QDs, which will allow us to choose the optimal QDs for the study.

Phase 2: It is an approach for the evaluation of treatments based on the nanolimes doped with the chosen QDs, enabling the evaluation of their applicability for cultural heritage and their effectiveness as consolidants for limestones.

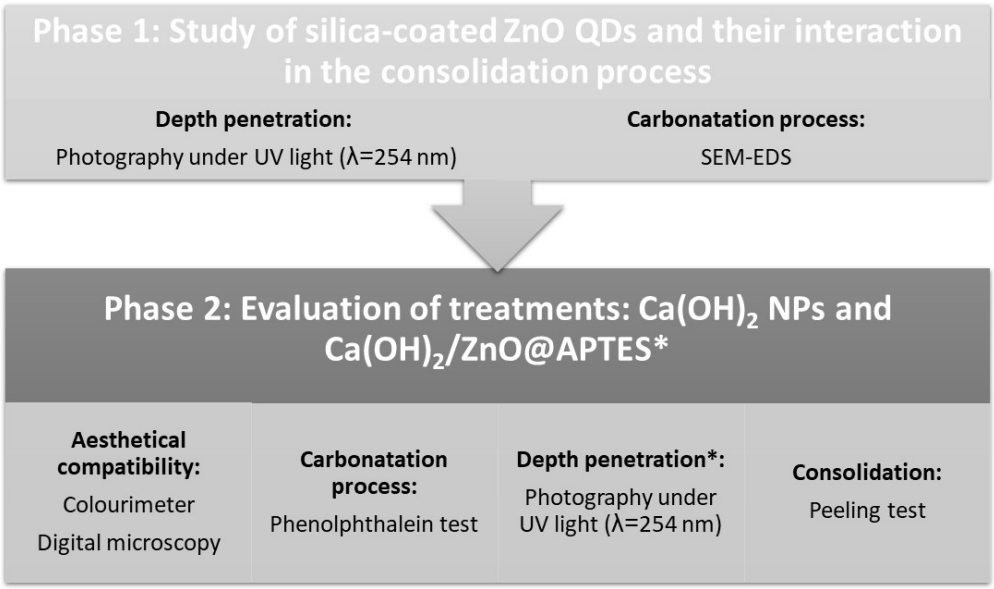

Fig. 1. Methodology of the evaluation of the treatments over stones.

2.4.1. Selection of the silica-coated ZnO QDs

The preliminary trial (phase 1 of Fig. 1) was designed to select the optimal silica-coated ZnO QDs and study their possible interference in the carbonatation process of nanolimes.

For this trial, limestone slabs (2.5 x 2.5 x 1 cm) from Puerto de Santa María were treated by $Ca(OH)_2$/ZnO@APTES and $Ca(OH)_2$/ZnO@TEOS at a concentration of 2.5 g nanolimes/L. The treatment was applied with a brush over the slab surfaces until it was apparently refused.

The depth penetration of treatments was measured in cross-sectional of slabs under UV light (λ=254 nm). The evaluation of the nanolime carbonatation was based on the generation of calcium carbonate in the samples [31]. SEM images were recorded in a GeminiSEM 300 microscope. Additionally, the effectiveness of the ZnO QDs as a tracer was studied by EDS. The EDS spectra were recorded by an Oxford Instruments Detector EDS X-Max 50.

2.4.2 Application on stone samples and evaluation of treatments

Limestone slabs (2.5 x 2.5 x 2.5 cm) were employed to analyse the penetration and consolidation properties of nanolimes (phase 2 of Fig. 1). For the trials, limestone slabs from the quarries of Puerto de Santa María and Espera (Cádiz, Spain) were chosen. These quarries were

172 used in the construction of important historical buildings in the south of Spain, such as the
173 Cathedral [21] or the Town Hall [20] of Seville.

174 The limestone from Puerto de Santa Maria (PSM) is a white-yellow biosparitic calcarenite,
175 which has a powdery appearance on the monument surfaces. This stone is made up
176 predominantly of carbonated and silica grains and a cement of calcite. The pore diameter of the
177 stone is between 10 and 100 μm according to Guerrero [20]. The limestone from Espera (ESP)
178 is a yellow biosparitic limestone with a homogeneous chemical composition based on calcite
179 and quartz. The stone has a pore diameter between 10 and 75 μm [20]. The open porosity of the
180 PSM and ESP stones was calculated according to UNE-EN 13755 [32] as 14.3% and 5.9%,
181 respectively. Additionally, their water absorption coefficient by the capillarity was also
182 calculated according to UNE-EN 1925 [33] as 179.3 and 38.6 $g/m^2.s^{0.5}$, respectively.

183 $Ca(OH)_2$ and $Ca(OH)_2$/ZnO@APTES were applied at a nanolime concentration of 2.5 g/L and
184 resuspended in five different solvents: water, ethanol, isopropanol, acetone and dipentene. The
185 quantity of the treatment was calculated using the criteria employed by Pinho and Mosquera
186 [34] for stone consolidates, where the product is applied until the surface's apparent refusal of
187 treatment. Consequently, the requirement of consolidation treatment was different between both
188 limestones, which was evident by their open porosity and absorption capacity, being 1.9 mL for
189 PSM slabs and 1 mL for ESP slabs. Four applications were carried out over each slab by
190 brushing on the treatment and allowing it to dry at room temperature (24°±2) for 20 days after
191 the last application. The assay was performed in triplicate.

192 The aesthetic compatibility was measured by colourimetry (colourimeter PCE-CSM 2, diameter
193 of circular measuring area: 8 mm, daylight illumination: D65). The chromatic variations (ΔE^*)
194 after treatments were calculated using the parameters defined by the CIELAB colour-system
195 according to equation 2.

196 $$\Delta E^* = \sqrt{\Delta L^{*2} + \Delta a^{*2} + \Delta b^{*2}} \qquad \text{Eq. 2}$$

where ΔL^*, Δa^* and Δb^* characterize the variations in the colour values from the controls in the black-white (brightness), red-green and yellow-blue axes, respectively. ΔL*, Δa*and Δb* were calculated as the variations between initial and final colour slabs.

After 20 days of drying, the limestone slabs were broken with a stone cutting machine into two halves. On one side, the ending of the carbonatation process was checked by a phenolphthalein test, and on the other side, the surface depth penetration of the treatments doped with ZnO QDs was observed under UV light. Additionally, the drying surface and cross-section samples were studied by a Zarbeco MiScope MP2 handheld digital microscope with 40 - 140X magnification lens.

The total carbonatation of the treatment was evaluated by the phenolphthalein test according to Borsoi et al. [35]. A solution of 1% phenolphthalein (60% ethanol-40% water) was nebulized over the cross-section of the samples after 20 days of the application of the treatments. Phenolphthalein is a common pH indicator that remains uncoloured for pH<8.2. In pH>9.8, the indicator colour changes to a purple colour. In this case, the presence of $Ca(OH)_2$ increases the pH beyond 11 and leads to the purple colour of the substrate. Nevertheless, the formation of the $CaCO_3$ remains uncoloured in the substrate due to it being a neutral compound.

The actual penetration of the $Ca(OH)_2$/ZnO@APTES treatments was observed in the cross-sectional samples with a UV lamp at 254 nm. The measurements were taken with an image processing program (ImageJ).

The consolidation of treated limestones was studied by the peeling test. This assay was carried out according to previously reported methods [36] using Scotch® Cristal tape (3 M) with 10 repetitions over the same location.

The percentage of consolidation (% Consolidation) relative to that of untreated samples was calculated according to equation 3.

$$\%\ \text{Consolidation} = \frac{\text{TRM untreated} - \text{TRM treated}}{\text{TRM untreated}} * 100 \qquad \text{Eq. 3}$$

where $TRM_{untreated}$ is the total removed material in the untreated sample and $TRM_{treated}$ is the total removed material in the treated sample.

3. Results and Discussion

3.1. Synthesis and characterization

The consolidation treatment based on nanolimes was selected to evaluate its penetration into the stone matrix. For that process, the $Ca(OH)_2$ nanoparticles were decorated with ZnO QDs, which have fluorescence in the UV wavelength. The nanocomposites that were synthesized form a white colloid that can be recovered easily by centrifugation (5000 rpm, 10 min) and resuspended in different solvents. In this case, the pellet was resuspended in isopropanol at the initial concentration of the commercial product (5 g nanolimes /L) for the nanoparticle conservation.

The $Ca(OH)_2$ nanoparticles of Nanorestore are hexagonal portlandite platelets with an average size of less than 100 nm, as determined by TEM [37,38]. Additionally, the ZnO QDs are spherical particles with an average size estimated at 7.7±1.4 nm by electron microscopy, which is consistent with the size of 8 nm described by Patra et al. [25]. Fig. 2A shows the hexagonal $Ca(OH)_2$ nanoparticle platelets according the description of Daniele et al. [9], which are decorated by tiny ZnO QDs with spheres shapes that were previously described by Patra et al. [25] and are distributed heterogeneously. The presence of Zn was corroborated by EDS (Fig. 2B) and also appeared in the peaks of the Si used in the stabilization process of the QD growth. After two days of drying, the rhombohedral crystals of calcite were observed with a medium size of 0.5-1 μm (Fig. 2C). This mineral is the most stable and least soluble calcium carbonate [31]. The calcium and zinc maps show that the ZnO QDs remain around the new crystals of calcite (Fig. 2D-E) and do not prevent the carbonatation process.

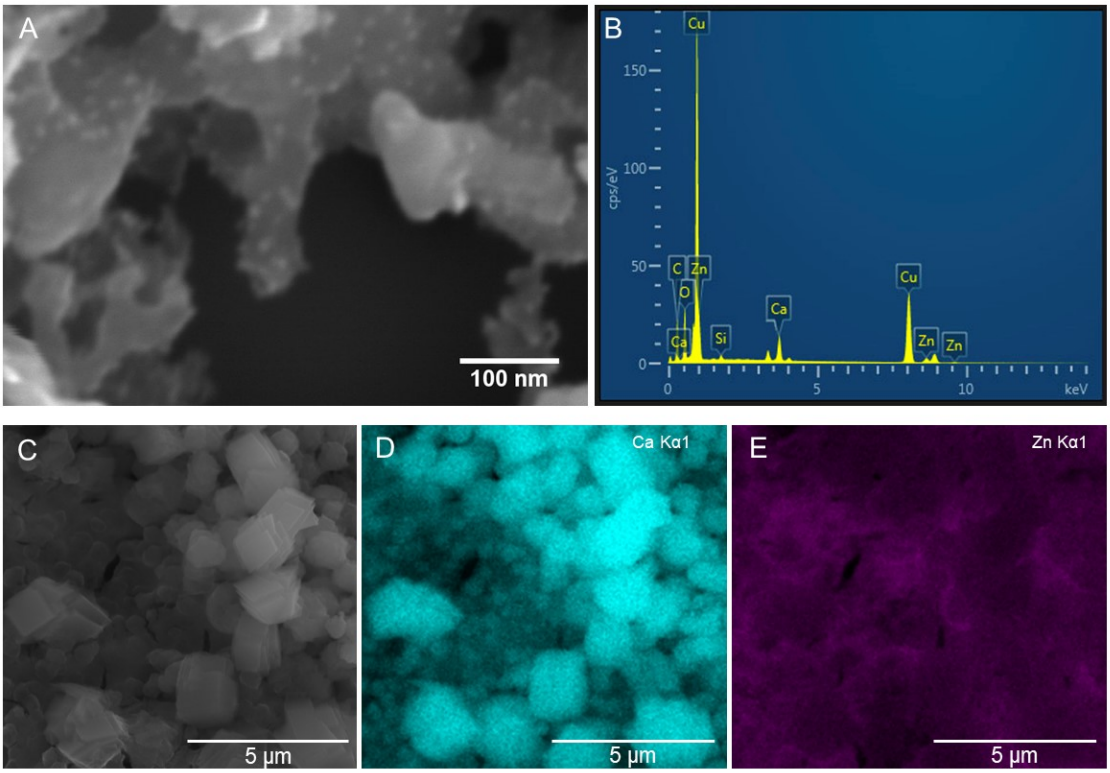

Fig. 2. SEM images of the $Ca(OH)_2$ nanoparticles decorated with ZnO QDs posed over a copper grid (A) and EDS spectra (B). The SEM image of $Ca(OH)_2$ nanoparticles decorated with ZnO QDs after one day of drying (C) and the EDS mapping of calcium and zinc (D and E, respectively) of that image.

Finally, the fluorescence of the ZnO QDs was studied in methanol. It has been reported that the broad emission from ZnO in the visible region is a spectrum of multiple emission bands originating from a variety of vacancies and interstitial defects on the surface and grain boundaries of ZnO [25,39]. Fig. 3 shows a broad emission spectrum that highlights the peaks at 483 and 525 nm that correspond to the blue and green regions, respectively. Patra et al. [25] suggest that the main peak in the green region could fluctuate between 510 and 534 nm as a function of the size of the QDs. The inset image in Fig. 3 shows the white-yellow fluorescence of the QDs under a UV light (λ=254 nm).

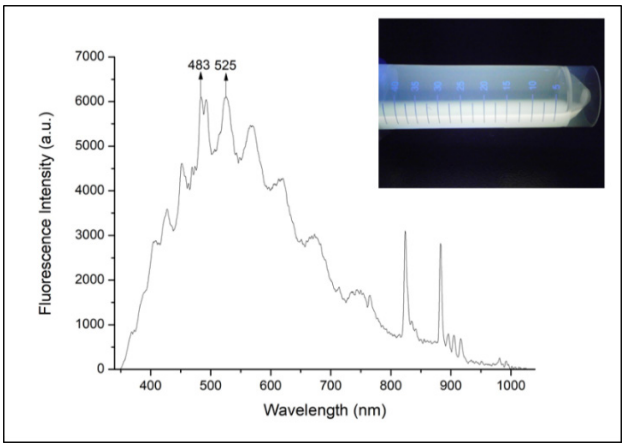

Fig. 3. Fluorescence emission spectra of ZnO QDs at the excitation wavelength from 250 to 900 nm by an arc of neon. The inset is an image of the fluorescence of the QDs at the wavelength of 254 nm.

3.2. Kinetic stability assay

The kinetic stability of the $Ca(OH)_2$ nanoparticles and $Ca(OH)_2$ nanoparticles decorated with ZnO QDs dispersed in different solvents (Table 1) was evaluated by turbidity measurements compared with the decantation process under visible and UV lights. In this way, the kinetic stability time was established for each dispersion.

The $Ca(OH)_2$ nanoparticles showed great stability in a wide range of the solvents (Table 2), especially in alcohols, dimethyl sulfoxide and dimethylformamide, for more than 48 hours. In contrast, these nanoparticles were very unstable in water, toluene and hexane, solvents that are classified as more polar (water) or non-polar (toluene, hexane) than the other solvents used. Salvadori and Dei [37] show that the low stability of the nanolimes in water is due to the lower effectiveness of the water as a peptizer. In fact, the absorption of solvent molecules onto the surfaces of nanolimes led to their subsequent stabilization [40].

The nanolimes doped with ZnO QDs had lower stability than did the non-doped nanolimes due to the modification of the nanoparticle surface with the QDs. The use of different silica coatings in the ZnO QDs showed remarkable differences between them. The use of (3-aminopropyl)trimethoxysilane (APTES) provided a great stability to the nanoparticles in

alcohols, dimethyl sulfoxide and dimethylformamide, while it decreased the stabilization in solvents with less polarity. The presence of tetraethylorthosilicate (TEOS) in the nanoparticles decreased their kinetic stability in all of the solvents except for octanol, in which the stability was above 48 hours. This different behaviour between these two silica-coatings could be due to the presence of amino groups on the surface of the ZnO@APTES QDs [41], while the presence only of methyl groups in the surface favoured a trend to agglomerate nanoparticles.

Table 2. Kinetic stability time expressed in hours (h)

	Solvent										
Nanoparticle	Water	Ethanol	Isopropanol	Octanol	Dimethyl sulfoxide	Dimethyl-formamide	Acetone	Ethyl acetate	Dipentene	Toluene	Hexane
$Ca(OH)_2$	0	>48	>48	>48	>48	>48	24	24	24	0	0
$Ca(OH)_2$/ZnO@APTES	0.5	>48	>48	24	>48	>48	0.5	0	0.5	0	0
$Ca(OH)_2$/ZnO@TEOS	0	24	0.5	>48	0.5	0.5	0	0.5	0.5	0	0.5

In general, the higher stability was obtained with alcohols (ethanol, isopropanol and octanol), which is in agreement with other studies [26,42,43]. The kinetic stability decreased with the increase in the solvent non-polarity. The exception was water, the most polar solvent analysed, where nanoparticles were not stable either according to the results found by Rodriguez-Navarro et al. [15] and Licchelli et al. [44].

Taking into consideration these results, we made the selection of solvents for the next assay (section 3.3.) by choosing a range of solvents with different capacities to maintain the $Ca(OH)_2$ nanoparticle stability. The chosen solvents were ethanol, isopropanol, dipentene, acetone and water, which are arranged from the highest to lowest kinetic stability of the solvent.

Moreover, all these solvents present a low toxicity for humans and the environment according to the time-weighted average (TWA) given by the National Institute for Occupational Safety and Health (NIOSH). Therefore, the solvents could be used by restorers for building or

archaeological stones. In this case, all the solvents have a TWA value greater than 400 ppm (Table 1), except for acetone (250 ppm).

3.3. Chromatography assays

A chromatography assay was carried out on $Ca(OH)_2$ decorated with ZnO QDs, and the measurement of the R_f was easy thanks to the fluorescence of the ZnO QDs under UV radiation (λ=254 nm).

One of the most important objectives of this assay was corroborated by the influence of the substrate composition in the solvent and its capability to shift the nanoparticles on the substrate. Until now, all the studies were focused on the nanoparticle-solvent interaction [17,26,43–46]. Nevertheless, it is necessary take into consideration a third factor, which is the substrate where the nanoparticle will be applied. As could be seen in Table 3, the R_f between silica gel (TLC-sheets Alugram® Sil) and mortar chromatographic substrate is different. The best R_f was achieved in mortar substrates with a composition similar to that of limestones. In fact, the presence of the silica-coating on the ZnO QDs made the resulting nanoparticles have a higher attraction to the silica gel substrate, which may be caused by the presence of methyl groups and the possibility to generate tight links with the substrate [47]. Thereby, the distance travelled by the nanoparticles decreased in comparison with that of the same product in the different chromatographic substrate (mortars), as seen in Table 3.

Table 3. Distance travelled relative to the solvent (R_f) as obtained by chromatography assays.

	$Ca(OH)_2$/ZnO@APTES					**$Ca(OH)_2$/ZnO@TEOS**				
Solvent	Water	Ethanol	Isopropanol	Acetone	Dipentene	Water	Ethanol	Isopropanol	Acetone	Dipentene
Silica gel (Alugram®)	0.12±0.01	0.11±0.01	0.23±0.04	0.10±0.01	0.06±0.01	0.13±0.01	0.12±0.01	0.10±0.01	0.07±0.01	0.32±0.01
Mortar	0.18±0.02	0.24±0.02	0.38±0.02	0.10±0.01	0.11±0.01	0.23±0.03	0.34±0.02	0.19±0.05	0.21±0.01	0.40±0.04

In general, the $Ca(OH)_2$/ZnO@TEOS nanoparticles showed higher R_f values than did the $Ca(OH)_2$/ZnO@APTES nanoparticles.

In the case of the $Ca(OH)_2$/ZnO@APTES nanoparticles, isopropanol suspensions displayed the best R_f in both the silica gel and mortar substrates, with R_f values of 0.23 and 0.38, respectively. The great kinetic stability of this dispersion (>48 hours) facilitates the chromatographic ascent of the nanoparticles shifted by solvents. In agreement with that assessment, the solvents with lower kinetic stability (water, acetone and dipentene) resulted in decreased R_f values (Table 3).

Against what was expected, the best R_f for $Ca(OH)_2$/ZnO@TEOS was obtained with a low-kinetic-stability solvent, dipentene (0.32 in silica gel and 0.4 in mortar substrate). Ethanol had a good result, while isopropanol considerably decreased the capability of the treatment to shift the nanoparticles compared to the results achieved by the $Ca(OH)_2$/ZnO@APTES nanoparticles.

In summary, this new approach helps to understand the behaviour of the nanolime dissolution in different substrates. If the affinity between the nanoparticles and substrate is high, then the chromatographic progression decreases. A good selection of the solvent considerably improves the R_f value, especially in the case of alcohols, which showed the highest kinetic stability.

3.4. Treatment evaluation

3.4.1. Selection of silica-coated ZnO QDs

Ethanol was used to carry out the selection of silica-coated ZnO QDs due to its great kinetic stability, which was 24 h for the TEOS-coated samples and more than 48 h for the APTES-coated samples, and its high R_f for both nanolimes, 0.34 and 0.24 for the TEOS- and APTES-coated samples, respectively.

As seen in Fig. 1, the first step was to measure the depth penetration of consolidants in the cross-sections of the limestone slabs. Fig.3 shows the real depth penetration of the treatments via the yellow fluorescence of the ZnO QDs. In the case of the $Ca(OH)_2$/ZnO@APTES

nanoparticles, the depth penetration was 1 cm (thickness of the slabs), while in $Ca(OH)_2$/ZnO@TEOS nanocomposites, it was slightly less at 0.85 cm.

The chemical analyses made by EDS evidenced the presence of Zn (ZnO QDs) along the cross-sectioned slabs (Fig. 4) for both nanoparticles. Moreover, the suitability of this UV method for the detection of the real penetration of nanoparticles was confirmed by detecting Zn in the consolidated areas.

In the samples treated with the $Ca(OH)_2$/ZnO@TEOS nanocomposites (Fig. 4 A), there appeared some calcite crystals, although some amorphous phases were appreciable, thus drawing out the carbonatation process and, consequently, decreasing the consolidation properties. The sample with $Ca(OH)_2$/ZnO@APTES nanoparticles (Fig. 4 B) indicates the finalization of the carbonatation process with the formation of rhombohedral crystal structures of calcite, which is in agreement with Rodriguez-Navarro [31].

The carbonatation process shows remarkable differences between the two silica-coated nanoparticle treatments. For this reason, $Ca(OH)_2$/ZnO@APTES nanoparticles were chosen to treat the stones in the following steps of this work.

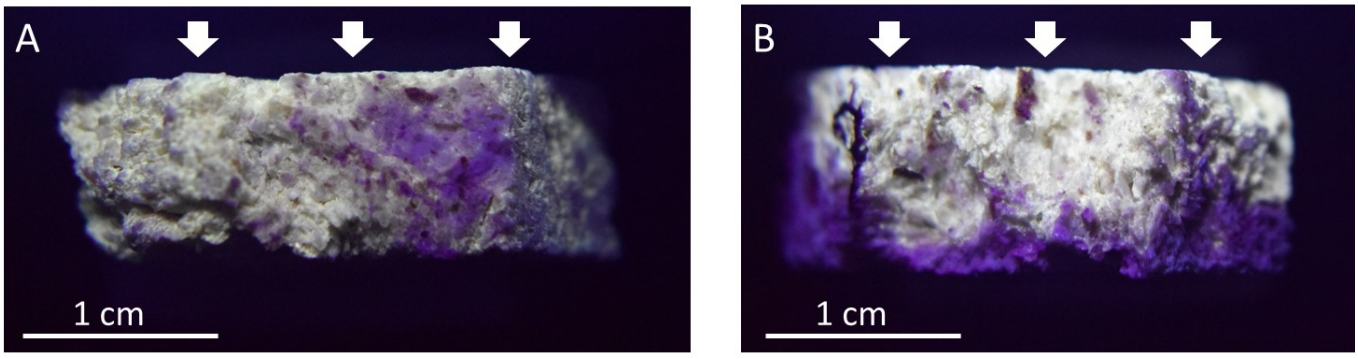

Fig. 3. Cross-section of limestones treated with $Ca(OH)_2$/ZnO@APTES (A) and $Ca(OH)_2$/ZnO@TEOS (B) under UV radiation (254 nm).

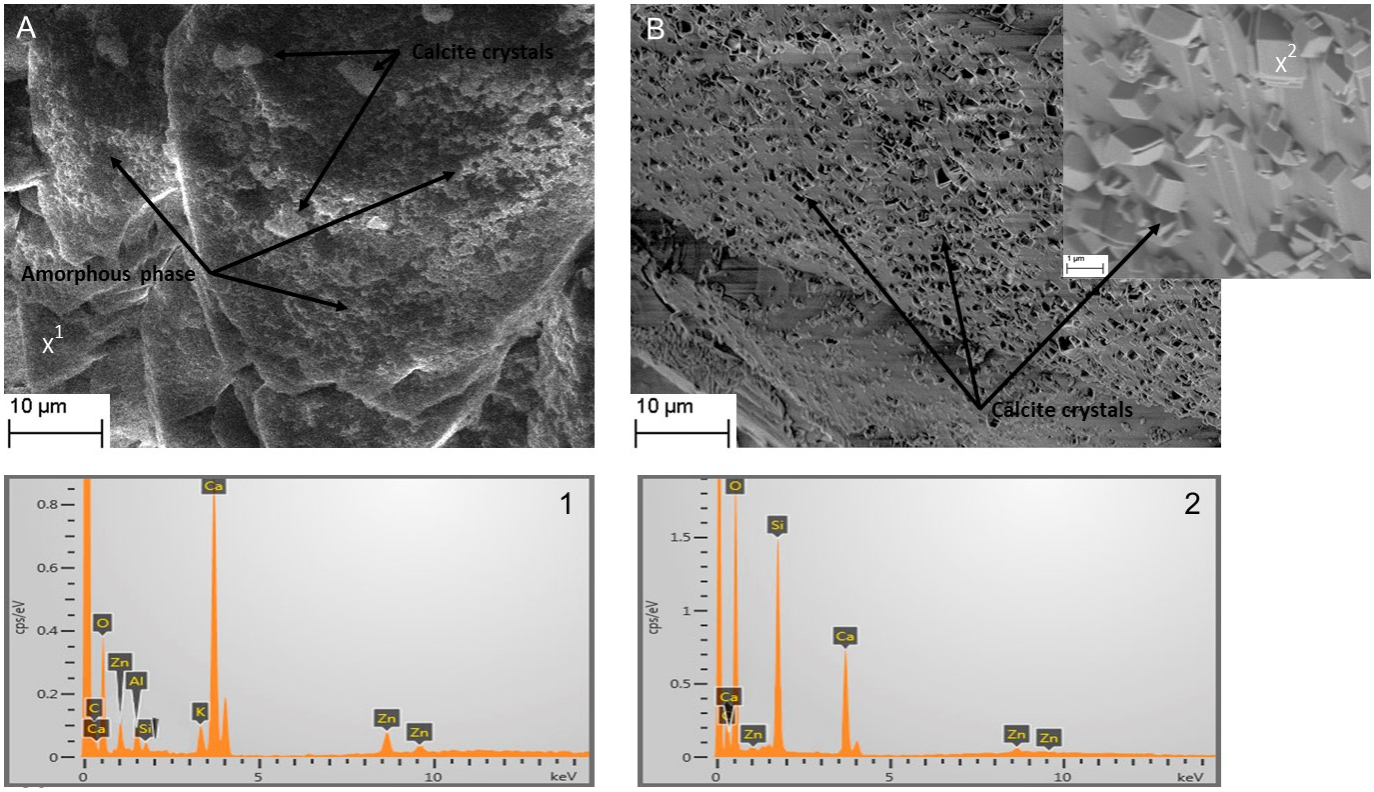

363 Fig 4. The SEM images of the treatments applied over PMS limestone after 20 days of drying.
364 (A) $Ca(OH)_2$/ZnO@TEOS nanoparticles. Point 1 corresponds to the EDS analysis. (B)
365 $Ca(OH)_2$/ZnO@APTES nanoparticles. Point 2 corresponds to the EDS analysis.

366 **3.4.2. Application on stone samples and evaluation of treatments**

367 The evaluation of the treatments was carried out by applying $Ca(OH)_2$/ZnO@APTES
368 nanoparticles over different limestones and comparing the results with those of commercial
369 nanolimes (Nanorestore®).

370 Aesthetical characteristics based on colour change must be analysed for the treatment evaluation
371 applied on cultural heritage sites. Although there are not clear standardized criteria for colour
372 changes, the most common criterion is that the treatment cannot change the colour by $\Delta E^*>5$
373 [48–50]. Other authors propose three ranges of chromatic changes for dyes in cultural heritage
374 porous materials: $\Delta E^*<5$, which is where chromatic changes cannot be detected by the human
375 eye; $5<\Delta E^*<10$, which is where chromatic changes can be detected by the human eye but are
376 still acceptable; and $\Delta E^*>10$, which is where chromatic changes are clearly visible [51–53].

377 Consequently, we classify optimal treatments as those with $\Delta E^*<5$ and acceptable treatments as
378 those with $5<\Delta E^*<10$.

379 In the case of the treatments applied over PSM limestone, the values of ΔE^* generally were
380 lower than 5 (Table 4) and consequently optimal for cultural heritage; the exceptions were the
381 applications in water or dipentene, where the high standard deviations showed the
382 heterogeneous behaviours of the treatments, and the ΔE^*s were 5.5 and 6, respectively. None of
383 the colour increments exceeded the value of 10, and so all treatments were acceptable. The least
384 pronounced colour changes were achieved by alcohol dispersions (approximately 2), without
385 remarkable differences between treatments. These good results are due to the high porosity of
386 this limestone (14.3%) and its large pore size (10-100 μm), which allowed a better depth
387 penetration of the treatments. No white haze was observed in the treated samples, as seen in the
388 example of the application in ethanol (Fig. 5A-C). Any remarkable difference could be
389 appreciated between the ΔE^* caused by the $Ca(OH)_2$/ZnO@APTES and $Ca(OH)_2$ nanoparticles
390 (Table 4).

391 In the ESP limestone, the ΔE^* values were higher, thus exceeding the value of 10 in several
392 occasions. This result was due to the physical properties of the stone, with a lower porosity
393 (5.9%) and lower range of porous size (10-75 μm). The accumulation of the treatment on the
394 surface produced a white haze, which is responsible for the higher colour changes. Fig. 5D-F
395 show the white haze generated after the application of the treatments suspended in ethanol. The
396 presence of ZnO QDs increased the white haze over the stone, which was amplified by the
397 increment of L* (brightness) and, consequently, the increased ΔE^* over 5. The treatment is not
398 the most advisable on surfaces that must be visible, although it would be acceptable on hidden
399 stone surfaces.

400

401

Table 4. Characterization of the limestone samples after the application of the different treatments.

	Puerto de Santa María (PSM)					Espera (ESP)				
	$Ca(OH)_2$		$Ca(OH)_2$/ZnO@APTES			$Ca(OH)_2$		$Ca(OH)_2$/ZnO@APTES		
Solvent	**ΔE***	% Consolidation[+]	**ΔE***	% Consolidation[+]	*Depth[++] (mm)*	**ΔE***	% Consolidation[+]	**ΔE***	% Consolidation[+]	*Depth[++] (mm)*
Water	**5.43±2.3**	89.07	**5.45±3.3**	82.52	*1.39±0.4*	**6.97±3.1**	24.09	**8.34±2.2**	45.77	*0.27±0.17*
Ethanol	**1.79±1.4**	61.30	**2.04±1.3**	92.29	*11.16±1.4*	**6.21±2.3**	50.72	**10.60±1.3**	31.18	*0.09±0.03*
Isopropanol	**2.29±1.9**	71.40	**1.98±0.2**	94.96	*9.65±0.1*	**7.48±1.9**	41.85	**11.66±4.4**	30.60	*0.28±0.22*
Acetone	**4.53±0.9**	53.49	**3.70±0.8**	93.74	*4.37±2.0*	**7.57±1.1**	17.64	**11.78±10.2**	24.60	*0.21±0.09*
Dipentene	**6.38±5.5**	59.75	**5.73±5.2**	94.12	*1.68±0.8*	**8.45±1.3**	59.43	**19.01±4.5**	17.64	*0.18±0.16*

[+]% of the grade of consolidation with respect to the untreated samples. Equation (Eq. 3) in section 2.6.
[++] Depth measures by fluorescence of ZnO@APTES QDs under UV radiation (256 nm).

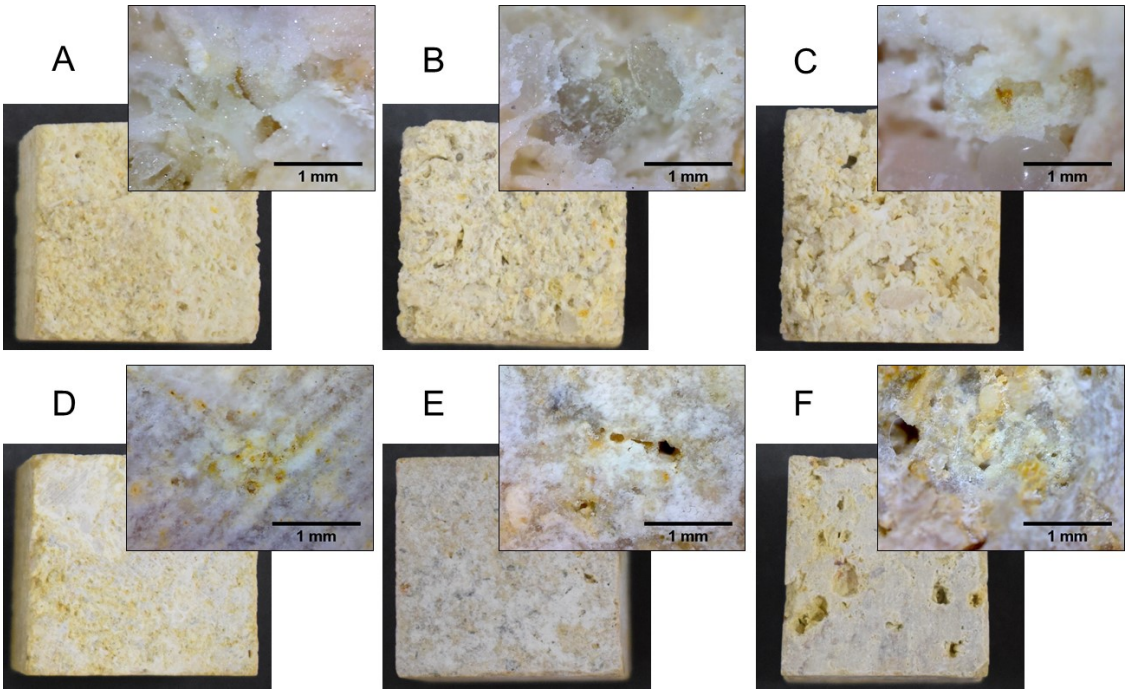

Fig. 5. Photography of limestone surfaces after the application of the different treatments with ethanol. Magnification of the surface (140 x) analysed by a Zarbeco handheld digital microscope. (A) Untreated PSM limestone. (B) $Ca(OH)_2$/ZnO@APTES applied over PSM limestone. (C) $Ca(OH)_2$ applied over PSM limestone. (D) Untreated ESP limestone. (E) $Ca(OH)_2$/ZnO@APTES applied over ESP limestone. (F) $Ca(OH)_2$ applied over ESP limestone.

The colour changes are related to the treatment penetration, and we observed that the lowest ΔE* was favoured by a good depth penetration of the treatments. The penetration depends on

texture of the stone and the solvent that is employed. The cross-section of the samples treated with the $Ca(OH)_2$/ZnO@APTES nanocomposites allows us to measure the real depth of the treatment under UV radiation (λ=254 nm). The suitability of the UV method for the detection of real penetration was confirmed in the preliminary trial by EDS, which detected Zn only in the consolidated areas. The penetration capability of the treatments is widely connected with the texture and porosity of the limestone and the solvent chosen. In this sense, the treatments that generated a homogeneous white layer over the surface of the ESP limestone had low penetration, as was evidenced by the UV light in the cross-section (Fig. 6F-I) in which the penetration thickness was a few micrometres (Table 4), and the values were closely related to the roughness of the stone, as can be deduced by the greater deviations of the penetration measurements. The superficial deposition of the treatments agrees with the highest ΔE* observed (higher than 10). On the other hand, the treatments had a noticeable penetration in PSM limestone according to the UV measurements (Fig 6B-D), thus achieving a depth penetration greater than 1 cm in alcohol dispersions, with the lowest colour increments (<2.3). The other solvents had depth penetration according to their colour increments, while water and dipentene had the worst depth penetration, approximately 1.5 mm. In conclusion, a good selection of the solvent allows one to improve the penetration of nanoparticles by more than 1 cm.

Table 4 shows the measurements of the depth penetration achieved by the different dispersions. The low surface tension of the alcohols (21 mN m^{-1}) and their good kinetic stability (>48 h) favoured a great penetration depth, especially in the case of ethanol, which reached a penetration of over 1.1 cm in PSM stone. This depth is even greater than those reached by other authors for nanolimes without QDs [7,9,44]. The water and dipentene solvents displayed the lowest penetration depths, although these solvents present a higher superficial tension (71.97 mN m^{-1} and 26.87 mN m^{-1}, respectively) and a lower viscosity (0.89 mPas and 0.92 mPas, respectively), which are characteristics that were exposed by Borsoy et al. [8] as critical to achieving a good penetration of a treatment by capillarity. In this case, the application methods

(brushing) conditioned the selection of the solvent with different physical properties, thus achieving greater results when the solvent has a low superficial tension, which is in agreement with Chelizzia et al. [11].

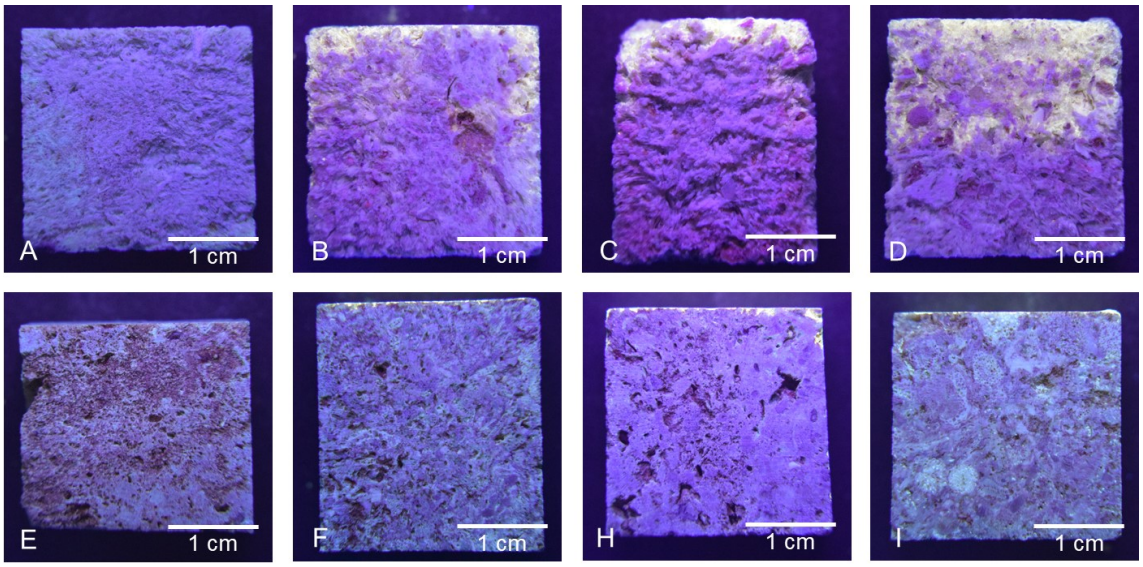

Fig. 6. Photography under UV radiation (254 nm) of the cross section of the samples treated with the $Ca(OH)_2$/ZnO@APTES nanocomposites that were suspended in different solvents. The first row corresponds to the PMS limestone and the second one to the ESP limestone. (A) Untreated. (B) Dipentene. (C) Acetone. (D) Ethanol. (E) Untreated. (F) Dipentene. (H) Acetone. (I) Ethanol.

Phenolphthalein tests were carried out over the cross-sectioned stones after 20 days of drying. The absence of the typical purple colour change by the reaction of the phenolphthalein at pH>9.8 established the total conversion of the nanolimes in calcite at pH values lower than 8.2.

The peeling test results indicated that the treatments increased the superficial cohesion of the treated limestones. The percentage of consolidation depended on the limestone (Table 4).

The ESP limestone presented less powdering. Despite that finding, the consolidation improved in 50% of the cases of nanolimes applied in dipentene and ethanol. In the case of the $Ca(OH)_2$/ZnO@APTES nanoparticles, the consolidation that was achieved was less, with the best results with water (46%). The rest of the solvents did not have remarkable consolidation in

458 this limestone, with some results lower than 30%, except for the nanolimes applied on
459 isopropanol.

460 In contrast, the consolidation achieved in the PSM limestone was very noticeable. All the
461 treatments reduced the powdering of this limestone by more than 50%, and this percentage was
462 increased to more than 80 in the case of $Ca(OH)_2$/ZnO@APTES. In this sense,
463 $Ca(OH)_2$/ZnO@APTES showed better results than those of the nanolimes alone. The best result
464 was obtained with isopropanol (95% of consolidation).

465 Figure 7 shows the evolution of different repetitions of the peeling assay. The typical trend is a
466 reduction in the amount of removed material in successive repetitions, which consequently
467 shows a decreasing linear progression. The gradient of this linear progression was more
468 pronounced in the decayed stones, such as the untreated PSM limestone in Fig. 7A. A good
469 consolidation of the stone decreases the removed material, and the gradient of the linear
470 progression tends to be a horizontal line. Those lines near the horizontal imply a homogeneous
471 state of conservation of the stone surface.

472 In the case of PSM limestone, the greater consolidation was obtained by
473 $Ca(OH)_2$/ZnO@APTES nanoparticles applied in the isopropanol dissolution, thus showing a
474 horizontal progression line in Fig. 7A (dotted lines). This good result with respect to
475 commercial $Ca(OH)_2$ nanoparticles is due to the slight presence of APTES, which increased the
476 consolidation property of the treatment and avoided the formation of typical microcracks that
477 are reported in some studies of the application of ethyl silicates on limestones [18]. In this
478 sense, the lack of APTES in the consolidation treatment lowered the effectiveness of the
479 treatment by 30%. In the case of the ESP limestone, the progression lines of the treatments are
480 similar to the untreated sample and display a lower capability to consolidate the material, which
481 may be due to this limestone having less damage by powdering.

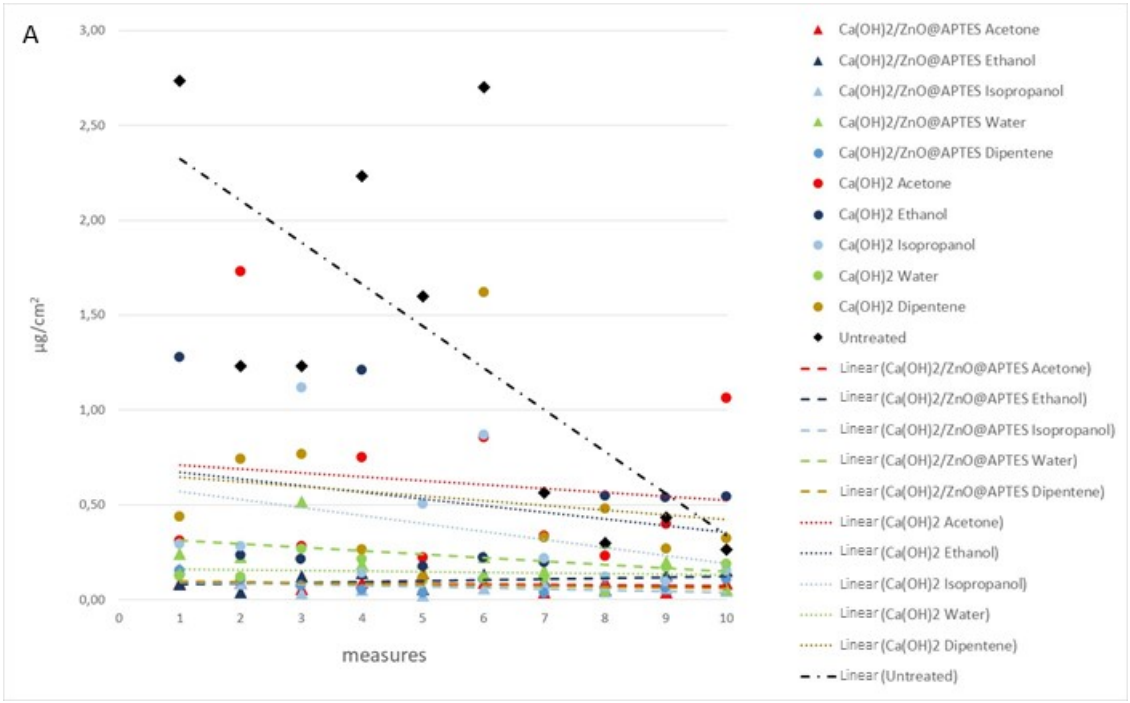

482

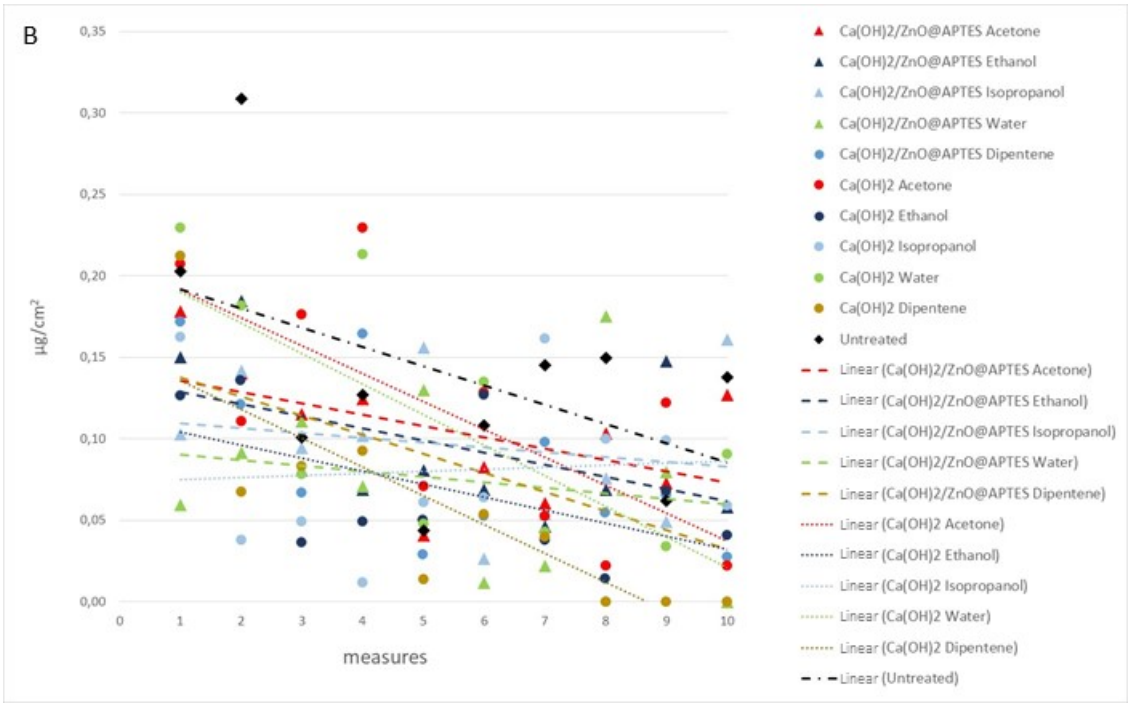

483

484 Fig. 7. Average of the peeling tests on Puerto de Santa María (A) and Espera (B) limestone after
485 the consolidation treatment and lineal progression lines.

486

487

Conclusions

Treatments based on nanolimes were evaluated as consolidants of limestones. One of the problems of this treatment is achieving a good depth penetration and avoiding the formation of white haze in the stone surfaces. For those purposes, the kinetic stability of dispersion with different solvents and the nanoparticle affinity for the solvents and the substrates were studied. The highest kinetic stabilities were obtained with alcohol solvents that, in general, had the highest distance travelled by the nanoparticles relative to the solvent in the chromatography assays.

Moreover, two different silica products were tested as stabilizers in the synthesis of the ZnO QDs, TEOS and APTES. The influence of the silica coatings in the consolidation properties of the nanolimes was researched. Although apparently both silica coatings had similar behaviours, the SEM images showed that the presence of TEOS favoured the formation of amorphous $CaCO_3$, while in the samples with $Ca(OH)_2$/ZnO@APTES nanoparticles, the SEM showed calcite crystals.

The trials in two different limestones allowed us to establish a third condition to take into consideration, the physical characteristics of the stone; this aspect was especially related to the porosity and pore size range of the stone. Based on the results of this study, to achieve a good penetration, the stone porosity should be greater than 14% with a predominantly high porous size. These characteristics allowed us to obtain good consolidation, as demonstrated by the decrease in colour changes, thus avoiding the formation of white haze on the stone surfaces.

The capability to measure the depth penetration of the treatment by the fluorescence of ZnO QDs was confirmed. The ZnO QDs remained on the nanolime surfaces without increasing in average size and showed a great fluorescence in the visible region under UV irradiation. These stable, nontoxic and low-cost QDs allowed us to conclude that the selection of the solvent is decisive in achieving a high depth penetration. As it was evaluated, the chosen solvents improved the depth penetration from a few millimetres (water) to more than 1 centimetre

514 (ethanol). This difference is related to the low superficial tension of the solvents and the high
515 kinetic stability of the dispersions when they are applied by brushing.

516 Finally, the consolidation effectiveness of nanolimes were improved with
517 $Ca(OH)_2$/ZnO@APTES nanoparticles. The consolidation achieved in high porous limestone
518 was greater than 90%. This treatment is a benefit for on-site works of restoration in cultural
519 heritage sites since the treatment can be controlled via UV radiation. Therefore, this method is
520 an easy, environmentally friendly and economical approach to establish a perceptible
521 consolidation treatment.

522 **Acknowledgements**

523 This study has been partially supported by the projects: BIA2015-64878-R (Art-Risk, RETOS
524 project of Ministerio de Economía y Competitividad and Fondo Europeo de Desarrollo
525 Regional), CTQ2013-48396-P (Ministerio de Economía y Competitividad and Fondo Europeo
526 de Desarrollo Regional) and the research teams TEP-199, P10-FQM-6615 and FQM-319 from
527 Junta Andalucía. J. Becerra is grateful to the Ministerio de Educación, Cultura y Deporte for his
528 pre-doctoral fellowship (FPU14/05348) and to the University Ecclesiastical Academy of
529 Thessaloniki for his stay as visiting researcher.

530 **References**

531 [1] G. B, R.H. Van, B. L, R. V, A.S. S, Nanolime deposition in Maastricht limestone : back-
532 migration or accumulation at the absorption surface?, in: EMABM 2015 Proc. 15th
533 Euroseminar Microsc. Appl. to Build. Mater. Delft, Netherlands, 17-19 June 2015, Delft
534 University of Technology, Delft, 2015: pp. 77–86.

535 [2] R. van Hees, R. Veiga, Z. Slížková, Consolidation of renders and plasters, Mater. Struct.
536 50 (2017) 65. doi:10.1617/s11527-016-0894-5.

537 [3] M. Favaro, R. Mendichi, F. Ossola, U. Russo, S. Simon, P. Tomasin, P.A. Vigato,
538 Evaluation of polymers for conservation treatments of outdoor exposed stone

monuments. Part I: Photo-oxidative weathering, Polym. Degrad. Stab. 91 (2006) 3083–3096. doi:10.1016/j.polymdegradstab.2006.08.012.

[4] S. Vicini, S. Margutti, G. Moggi, E. Pedemonte, In situ copolymerisation of ethylmethacrylate and methylacrylate for the restoration of stone artefacts, J. Cult. Herit. 2 (2001) 143–147. doi:10.1016/S1296-2074(01)01114-1.

[5] E. Sassoni, S. Naidu, G.W. Scherer, The use of hydroxyapatite as a new inorganic consolidant for damaged carbonate stones, J. Cult. Herit. 12 (2011) 346–355. doi:10.1016/j.culher.2011.02.005.

[6] P. Baglioni, D. Chelazzi, R. Giorgi, E. Carretti, N. Toccafondi, Y. Jaidar, Commercial Ca(OH)2 nanoparticles for the consolidation of immovable works of art, Appl. Phys. A Mater. Sci. Process. 114 (2014) 723–732. doi:10.1007/s00339-013-7942-6.

[7] L. Dei, B. Salvadori, Nanotechnology in cultural heritage conservation: nanometric slaked lime saves architectonic and artistic surfaces from decay, J. Cult. Herit. 7 (2006) 110–115. doi:10.1016/j.culher.2006.02.001.

[8] G. Borsoi, B. Lubelli, R. van Hees, R. Veiga, A.S. Silva, Understanding the transport of nanolime consolidants within Maastricht limestone, J. Cult. Herit. 18 (2016) 242–249. doi:10.1016/j.culher.2015.07.014.

[9] V. Daniele, G. Taglieri, R. Quaresima, The nanolimes in Cultural Heritage conservation: Characterisation and analysis of the carbonatation process, J. Cult. Herit. 9 (2008) 294–301. doi:10.1016/j.culher.2007.10.007.

[10] R. Giorgi, M. Ambrosi, N. Toccafondi, P. Baglioni, Nanoparticles for cultural heritage conservation: Calcium and barium hydroxide nanoparticles for wall painting consolidation, Chem. - A Eur. J. 16 (2010) 9374–9382. doi:10.1002/chem.201001443.

[11] D. Chelazzi, G. Poggi, Y. Jaidar, N. Toccafondi, R. Giorgi, P. Baglioni, Hydroxide nanoparticles for cultural heritage: Consolidation and protection of wall paintings and

carbonate materials, J. Colloid Interface Sci. 392 (2013) 42–49. doi:10.1016/j.jcis.2012.09.069.

[12] R. Giorgi, L. Dei, P. Baglioni, A New Method for Consolidating Wall Paintings Based on Dispersions of Lime in Alcohol, Stud. Conserv. 45 (2000) 154–161. doi:10.1179/sic.2000.45.3.154.

[13] I. Natali, M.L. Saladino, F. Andriulo, D. Chillura Martino, E. Caponetti, E. Carretti, L. Dei, Consolidation and protection by nanolime: Recent advances for the conservation of the graffiti, Carceri dello Steri Palermo and of the 18th century lunettes, SS. Giuda e Simone Cloister, Corniola (Empoli), J. Cult. Herit. 15 (2014) 151–158. doi:10.1016/j.culher.2013.03.002.

[14] G. Taglieri, V. Daniele, G. Rosatelli, S. Sfarra, M.C. Mascolo, C. Mondelli, Eco-compatible protective treatments on an Italian historic mortar (XIV century), J. Cult. Herit. 25 (2017) 135–141. doi:10.1016/J.CULHER.2016.12.008.

[15] C. Rodriguez-Navarro, A. Suzuki, E. Ruiz-Agudo, Alcohol Dispersions of Calcium Hydroxide Nanoparticles for Stone Conservation, Langmuir. 29 (2013) 11457–11470. doi:10.1021/la4017728.

[16] D. Costa, J.D. Rodrigues, Consolidation of a porous limestone with nanolime, 12th Int. Congr. Deterior. Conserv. Stone. (2013).

[17] G. Taglieri, J. Otero, V. Daniele, G. Gioia, L. Macera, V. Starinieri, A.E. Charola, The biocalcarenite stone of Agrigento (Italy): Preliminary investigations of compatible nanolime treatments, J. Cult. Herit. 30 (2018) 92–99. doi:10.1016/J.CULHER.2017.11.003.

[18] G. Borsoi, M. Tavares, R. Veiga, A.S. Silva, Microstructural Characterization of Consolidant Products for Historical Renders: An Innovative Nanostructured Lime Dispersion and a More Traditional Ethyl Silicate Limewater Solution, Microsc.

589 Microanal. 18 (2012) 1181–1189. doi:10.1017/S1431927612001341.

590 [19] G. Borsoi, B. Lubelli, R. van Hees, R. Veiga, A. Santos Silva, Evaluation of the
591 effectiveness and compatibility of nanolime consolidants with improved properties,
592 Constr. Build. Mater. 142 (2017) 385–394. doi:10.1016/j.conbuildmat.2017.03.097.

593 [20] M.A. Guerrero, Diagnóstico del estado de alteración de la piedra del Palacio Consistorial
594 de Sevilla. Causas y mecanismos, Universidad de Sevilla (Spain), 1990.

595 [21] M.Á. Bello López, Caracterización y estado de alteración química de los materiales
596 empleados en la construción de la Catedral de Sevilla, Univerisdad de Sevilla, 1988.

597 [22] D. Millers, L. Grigorjeva, W. Łojkowski, T. Strachowski, Luminescence of ZnO
598 nanopowders, Radiat. Meas. 38 (2004) 589–591.
599 doi:10.1016/J.RADMEAS.2004.05.001.

600 [23] K. Matsuyama, Y. ki Maeda, T. Matsuda, T. Okuyama, H. Muto, Formation of
601 poly(methyl methacrylate)-ZnO nanoparticle quantum dot composites by dispersion
602 polymerization in supercritical CO2, J. Supercrit. Fluids. 103 (2015) 83–89.
603 doi:10.1016/j.supflu.2015.04.025.

604 [24] Y. Zhang, T.R. Nayak, H. Hong, W. Cai, Biomedical applications of zinc oxide
605 nanomaterials., Curr. Mol. Med. 13 (2013) 1633–45.
606 http://www.ncbi.nlm.nih.gov/pubmed/24206130 (accessed July 15, 2018).

607 [25] M.K. Patra, M. Manoth, V.K. Singh, G. Siddaramana Gowd, V.S. Choudhry, S.R.
608 Vadera, N. Kumar, Synthesis of stable dispersion of ZnO quantum dots in aqueous
609 medium showing visible emission from bluish green to yellow, J. Lumin. 129 (2009)
610 320–324. doi:10.1016/j.jlumin.2008.10.014.

611 [26] G. Borsoi, B. Lubelli, R. van Hees, R. Veiga, A.S. Silva, Optimization of nanolime
612 solvent for the consolidation of coarse porous limestone, Appl. Phys. A. 122 (2016) 846.
613 doi:10.1007/s00339-016-0382-3.

614 [27] A. Wypych, Databook of Solvents, ChemTec Publishing, Toronto, 2014.

615 [28] C. Reichardt, Empirical Parameters of Solvent Polarity as Linear Free-Energy
616 Relationships, Angew. Chemie Int. Ed. English. 18 (1979) 98–110.
617 doi:10.1002/anie.197900981.

618 [29] PubChem, The PubChem Project, (2017). https://pubchem.ncbi.nlm.nih.gov/ (accessed
619 May 21, 2018).

620 [30] L. Masschelein-Kleiner, Los solventes (The Solvents), Centro Nacional de Conservación
621 y Restauración DIBAM, Santiago de Chile, 2004.

622 [31] C. Rodriguez-Navarro, K. Elert, R. Ševčík, Amorphous and crystalline calcium
623 carbonate phases during carbonation of nanolimes: Implications in heritage conservation,
624 CrystEngComm. 18 (2016) 6594–6607. doi:10.1039/c6ce01202g.

625 [32] British Standards Institution., Natural stone test methods : determination of water
626 absorption at atmospheric pressure., British Standards Institution, 2008.

627 [33] AENOR, UNE-EN 1925, Natural Stone test methods. Determination of water absorption
628 coefficient by capillarity, (1999).

629 [34] L. Pinho, M.J. Mosquera, Photocatalytic activity of TiO2-SiO2 nanocomposites applied
630 to buildings: Influence of particle size and loading, Appl. Catal. B Environ. 134–135
631 (2013) 205–221. doi:10.1016/j.apcatb.2013.01.021.

632 [35] G. Borsoi, B. Lubelli, R. van Hees, R. Veiga, A. Santos Silva, Application Protocol for
633 the Consolidation of Calcareous Substrates by the Use of Nanolimes: From Laboratory
634 Research to Practice, Restor. Build. Monum. 0 (2017). doi:10.1515/rbm-2016-0008.

635 [36] M. Drdácký, J. Lesák, S. Rescic, Z. Slížková, P. Tiano, J. Valach, Standardization of
636 peeling tests for assessing the cohesion and consolidation characteristics of historic stone
637 surfaces, Mater. Struct. 45 (2012) 505–520. doi:10.1617/s11527-011-9778-x.

[37] B. Salvadori, L. Dei, Synthesis of Ca(OH)2 nanoparticles from diols, Langmuir. 17 (2001) 2371–2374. doi:10.1021/la0015967.

[38] L.S. Gomez-Villalba, P. López-Arce, A. Zornoza, M. Álvarez de Buergo, R. Fort, Evaluación del tratamiento de consolidación de dolomías mediante nanopartículas de hidróxido de calcio en condiciones de alta humedad relativa, Bol. La Soc. Esp. Ceram. y Vidr. 50 (2011) 85–92. doi:10.3989/cyv.122011.

[39] A.M. Pourrahimi, D. Liu, V. Ström, M.S. Hedenqvist, R.T. Olsson, U.W. Gedde, Heat treatment of ZnO nanoparticles: new methods to achieve high-purity nanoparticles for high-voltage applications, J. Mater. Chem. A. 3 (2015) 17190–17200. doi:10.1039/c5ta03120f.

[40] E. Fratini, M.G. Page, R. Giorgi, H. Cölfen, P. Baglioni, B. Demé, T. Zemb, Competitive surface adsorption of solvent molecules and compactness of agglomeration in calcium hydroxide nanoparticles, Langmuir. 23 (2007) 2330–2338. doi:10.1021/la062023i.

[41] N. Chekina, D. Horák, P. Jendelová, M. Trchová, M.J. Beneš, M. Hrubý, V. Herynek, K. Turnovcová, E. Syková, Fluorescent magnetic nanoparticles for biomedical applications, J. Mater. Chem. 21 (2011) 7630. doi:10.1039/c1jm10621j.

[42] M. Ambrosi, L. Dei, R. Giorgi, C. Neto, P. Baglioni, Stable dispersions of Ca(OH)2 in aliphatic alcohols : properties and application in cultural heritage conservation, Prog. Colloid Polym. Sci. 118 (2001) 68–72. doi:10.1007/3-540-45725-9_15.

[43] C. Rodriguez-Navarro, I. Vettori, E. Ruiz-Agudo, Kinetics and Mechanism of Calcium Hydroxide Conversion into Calcium Alkoxides: Implications in Heritage Conservation Using Nanolimes, Langmuir. 32 (2016) 5183–5194. doi:10.1021/acs.langmuir.6b01065.

[44] M. Licchelli, M. Malagodi, M. Weththimuni, C. Zanchi, Nanoparticles for conservation of bio-calcarenite stone, Appl. Phys. A Mater. Sci. Process. 114 (2014) 673–683.

663 doi:10.1007/s00339-013-7973-z.

664 [45] C. Rodriguez-Navarro, E. Ruiz-Agudo, M. Ortega-Huertas, E. Hansen, Nanostructure
665 and irreversible colloidal behavior of Ca(OH) 2: Implications in cultural heritage
666 conservation, Langmuir. 21 (2005) 10948–10957. doi:10.1021/la051338f.

667 [46] G. Poggi, N. Toccafondi, D. Chelazzi, P. Canton, R. Giorgi, P. Baglioni, Calcium
668 hydroxide nanoparticles from solvothermal reaction for the deacidification of degraded
669 waterlogged wood, J. Colloid Interface Sci. 473 (2016) 1–8.
670 doi:10.1016/j.jcis.2016.03.038.

671 [47] R. Snethlage, Stone Conservation, in: S. Siegesmund, R. Snethlage (Eds.), Stone Archit.,
672 5th ed., Springer Berlin Heidelberg, Berlin, Heidelberg, 2014: pp. 415–550.
673 doi:10.1007/978-3-642-45155-3.

674 [48] L. Pinho, M. Rojas, M.J. Mosquera, Ag–SiO2–TiO2 nanocomposite coatings with
675 enhanced photoactivity for self-cleaning application on building materials, Appl. Catal.
676 B Environ. 178 (2015) 144–154. doi:10.1016/j.apcatb.2014.10.002.

677 [49] P. Sanmartín, F. Villa, A. Polo, B. Silva, B. Prieto, F. Cappitelli, Rapid evaluation of
678 three biocide treatments against the cyanobacterium Nostoc sp. PCC 9104 by color
679 changes, Ann. Microbiol. 65 (2015) 1153–1158. doi:10.1007/s13213-014-0882-3.

680 [50] L. Graziani, E. Quagliarini, M. D'Orazio, The role of roughness and porosity on the self-
681 cleaning and anti-biofouling efficiency of TiO2-Cu and TiO2-Ag nanocoatings applied
682 on fired bricks, Constr. Build. Mater. 129 (2016) 116–124.
683 doi:10.1016/j.conbuildmat.2016.10.111.

684 [51] O. García, K. Malaga, Definition of the procedure to determine the suitability and
685 durability of an anti-graffiti product for application on cultural heritage porous materials,
686 J. Cult. Herit. 13 (2012) 77–82. doi:10.1016/j.culher.2011.07.004.

687 [52] P. Ortiz, V. Antúnez, R. Ortiz, J.M.M. Martín, M.A.A. Gómez, A.R.R. Hortal, B.

688 Martínez-Haya, Comparative study of pulsed laser cleaning applied to weathered marble
689 surfaces, Appl. Surf. Sci. 283 (2013) 193–201. doi:10.1016/j.apsusc.2013.06.081.

690 [53] J. Becerra, A.P. Zaderenko, M.J. Sayagués, R. Ortiz, P. Ortiz, Synergy achieved in
691 silver-TiO 2 nanocomposites for the inhibition of biofouling on limestone, Build.
692 Environ. 141 (2018) 80–90. doi:10.1016/j.buildenv.2018.05.020.

693